Ultrasonics Sonochemistry 77 (2021) 105674

Contents lists available at ScienceDirect

Ultrasonics Sonochemistry

journal homepage: www.elsevier.com/locate/ultson

Study on the formation mechanism of isoniazid crystal defects and defect elimination strategy based on ultrasound

Min Li [a,b], Weiguo Hu [d], Lingyu Wang [a,b], Jiahao Wei [a,b], Jingjing Sun [a,b], Jiahui Li [a,b], Dandan Han [a,b,*], Junbo Gong [a,b,c]

[a] School of Chemical Engineering and Technology, State Key Laboratory of Chemical Engineering, Tianjin University, Tianjin 300072, People's Republic of China
[b] The Co-Innovation Center of Chemistry and Chemical Engineering of Tianjin, Tianjin 300072, People's Republic of China
[c] Chemistry and Chemical Engineering Guangdong Laboratory, Shantou 515031, People's Republic of China
[d] North China Pharmaceutical Group Co., Ltd., Shijiazhuang, People's Republic of China

ARTICLE INFO

Keywords:
Crystal defect
Isoniazid
Molecular simulation
Ultrasound
Defect elimination

ABSTRACT

In crystallization, crystal growth defects may reduce the strength and purity of crystals, which are not welcomed in the industry. Herein, isoniazid (INH) crystals were chosen as an example to investigate the formation of crystal defects at the molecular scale by combining experiments and molecular dynamics simulations. It was found that the strong interaction between the solvent and the crystal surface, high temperature, small stirring rate, and low supersaturation can lead to more pronounced crystal defects. The bulk severity of INH crystal defects was reflected by N_2 adsorption–desorption measurement. Besides, the single-crystal growth experiments manifested the rough growth mechanism for the (1 1 0) surface in the axial direction and the stepwise growth mechanism for the (0 0 2) surface in the radial direction. For the (1 1 0) surface, cavities occurred under the condition where the growth rate of the crystal edges and corners was greater than that of the surface center due to the starvation phenomenon of diffusion. While for the (0 0 2) surface, when the solvent removal rate was lower than the solute insertion rate, liquid inclusions were formed, which was verified by Raman microscopy. Furthermore, the ultrasonic strategy was successfully proposed to eliminate INH crystal defects and prepare perfect INH crystals. Moreover, the mechanism of ultrasound to reduce the crystal defect was proposed. We believe this work can provide insights into the design and preparation of defect-free crystals in crystallization.

1. Introduction

Crystal defects refer to the region where the arrangement of the crystal deviates from the ideal structure [1,2]. In industrial crystallization, defects in organic crystals are usually harmful to the mechanical property and purity of crystal products [3]. Therefore, it is meaningful to figure out the formation mechanism of crystal defects to make perfect crystals.

In general, crystal defects can be divided into micro defects and macroscopic defects [4,5]. Microscopic defects refer to dislocations, vacancies, interstitial atoms, etc., which often exist in metallic materials [6,7], and affect the performance of crystals [8,9]. Macroscopic crystal defects include cavities, inclusions, etc., which are widely found in organic compounds [10–12]. Since 1966 Denbigh et al. [13] studied the liquid inclusions of hexamethylenetetramine, more research has been focused on macroscopic crystal defects in organic crystals during the solution crystallization process [14,15]. The liquid inclusions can eventually lead to macroscopic holes, cavities, etc., which significantly decrease the purity and stability of organic crystals and even cause drug degradation and agglomeration. Waldschmidt et al. [16,17] have proposed that the liquid inclusions and cavities inside the ciclopirox crystals obtained by recrystallization in ethyl acetate originated from the trapping of the mother liquor during the diffusion of crystal growth. Besides, Sun et al. [18] have proposed that growth cavities in vinpocetine crystals were formed spontaneously due to the staving phenomenon of diffusion.

Overall, the formation of crystal defects does not proceed through a single mechanism and the reasons for the formation of liquid inclusions and cavities are complicated. So, exploring one general defect formation mechanism is urgent to guide the elimination of crystal defects.

* Corresponding author at: School of Chemical Engineering and Technology, State Key Laboratory of Chemical Engineering, Tianjin University, Tianjin 300072, People's Republic of China; The Co-Innovation Center of Chemistry and Chemical Engineering of Tianjin, Tianjin 300072, People's Republic of China.
E-mail address: handandan@tju.edu.cn (D. Han).

https://doi.org/10.1016/j.ultsonch.2021.105674
Received 8 June 2021; Received in revised form 10 July 2021; Accepted 13 July 2021
Available online 19 July 2021

For solution crystallization, modulation of crystal parameters, such as temperature, stirring rate, and supersaturation, can be one general strategy to eliminate crystal defects, but sometimes it lacks effectiveness or costs much [19]. On the other hand, solution ultrasound is an effective method for the control of the particle size, morphology, and polymorphism of crystals [20–22]. Besides, as one intensified crystallization method [23], ultrasound can be applied to obtain crystals with few defects. For example, Yu et al. [19] have successfully obtained perfect vinpocetine crystals by an adjustable power bath ultrasonic generator at a power of about 30 W. However, the ultrasonic strategy to eliminate crystal defects is not widely applied [24], which needs to be explored for reducing crystal defects effectively.

Isoniazid (INH, CAS Registry No. 54–85-3), an active pharmaceutical ingredient (API), is regarded as the first-line anti-tuberculosis drug [25]. Crystallization is the key process for the purification of INH and determines its final crystal performance. However, we have found that INH appeared crystal defects in isopropanol (Fig. 1), which may affect the purity of INH and its subsequent downstream operations, such as milling, tableting, and storage. Therefore, it is of great significance to study the formation mechanism of INH defects to obtain crystals with perfect morphology.

Hence, the main purpose of this research is as follows. First, the roles of the solvent, supersaturation, temperature, and stirring rate on INH crystal defects were investigated by batch crystallization. Second, the growth mechanism of INH was revealed through single crystal growth experiments. Third, the formation mechanism of INH crystal defects was disclosed through the analysis of molecular simulation and experiments, where powder X-ray diffraction, scanning electronic microscopy, Raman microscopy, N_2 adsorption–desorption measurement, and the morphologi G3 were employed. Fourth, ultrasound-assisted crystallization was carried out to obtain defect-free INH crystals with great morphology.

2. Materials and methods

2.1. Materials

INH crystals (mass purity: 99.0%) were supplied by Wuhan Dongkangyuan Technology Co., Ltd (Wuhan, China). The organic solvents (mass purity: 99.5%), methanol, ethanol, and isopropanol were bought from Rionlon Bohua Pharmaceutical & Chemical Co., Ltd (Tianjin, China). All the reagents were used without further purification.

2.2. Characterization

2.2.1. Optical Microscopy

INH crystal morphology was observed by optical microscopy (Olympus U-CMAD3, Japan). The size of the growing crystal seed was measured by using an optical polarizing microscope (Eclipse E200, Nikon) at regular time intervals.

2.2.2. Scanning electron microscopy (SEM)

INH crystal morphology was characterized by the scanning electron microscope (SEM, TM3000, Hitachi Co., Japan) operating at 15 kV under vacuum. The samples were immobilized with the carbon conductive adhesive on an aluminum holder and then coated with gold for conductivity before scanning.

2.2.3. Raman Microscopy

The composition of defects (liquid inclusions) was analyzed by Raman microscopy (DXR Raman Microscope, American Thermal Power Company). The excitation of Raman scattering was operated by a He–Ne laser at a wavelength of 532 nm and through the microscope objective × 50 LWF with spectral resolution (1.496 cm^{-1}). Measurement was performed under the range of 50–3500 cm^{-1}. The sample was exposed 5 times and 7 s for each.

2.2.4. PXRD determination

Powder X-ray diffraction (PXRD) was used to identify the polymorphic forms of INH. The D/max-2500 X-ray diffractometer (Rigaku, Japan) was operated at 40 kV and 100 mA using Cu Kα radiation (1.5405 Å) with a step size of 2 θ and a dwell time of 1 s scanning from 2° to 30° identified.

2.2.5. N2 adsorption–desorption measurement

The content of macro defects was quantitively reflected by the N_2 adsorption–desorption measurement using an Automated Gas Sorption analyzer (Quantachrome Instruments, Autosorb-IQ).

2.3. The batch cooling crystallization

The batch crystallization was performed to study the solvent, supersaturation, temperature, stirring rate effects on INH crystal defects. For each experiment, one temperature controller (Type, CF41, Julabo Technology Co., Ltd) was set to the growth temperature T_1 and another temperature controller was set to the dissolution temperature T_2. For every process, a known amount of INH crystals were added to the crystallizer to make a supersaturated solution according to the solubility. Note that the supersaturation (S) in this work was defined as the concentration of a solution divided by the solubility. And then the solution was heated to the dissolution temperature T_2 to get the solution well dissolved. After that, the solution was quenching cooled to the growth temperature T_1 to grow the INH crystals. It has been measured that the solution could reach the growth temperature in 2 mins, and then the nucleation occurred. Moreover, the details about the operating parameters are listed in Table 1, and the corresponding results will be discussed later.

2.4. Molecular simulation

2.4.1. Theory

The attachment energy (AE) model is widely applied in the prediction of crystal morphology by the simulation calculation of the attachment energy [26,27]. The lower the absolute attachment energy support for the lower growth rate, and the relative growth rate of the (*h k l*) face

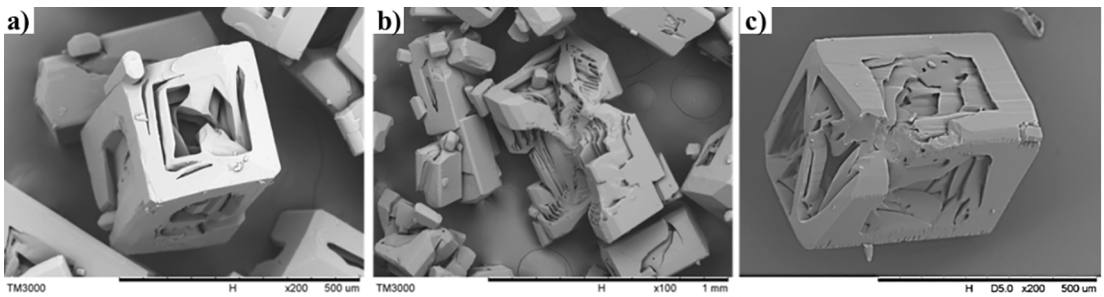

Fig. 1. INH crystals with defects in isopropanol (three different views).

Table 1
The operating parameters for batch cooling crystallization.

Experiment	Solvent type	Growth Temperature(T_1)	Supersaturation(S)	Stirring rate(r)	Dissolution temperature(T_2)
E1	Methanol	298.15 K	1.5	300 rpm	323.15 K
E2	Ethanol	298.15 K	1.5	300 rpm	323.15 K
E3	Isopropanol	298.15 K	1.5	300 rpm	323.15 K
E4	Isopropanol	298.15 K	2.0	300 rpm	323.15 K
E5	Isopropanol	298.15 K	2.5	300 rpm	323.15 K
E6	Isopropanol	298.15 K	1.5	500 rpm	323.15 K
E7	Isopropanol	298.15 K	1.5	800 rpm	323.15 K
E8	Isopropanol	283.15 K	1.5	300 rpm	308.15 K
E9	Isopropanol	313.15 K	1.5	300 rpm	338.15 K

E1, E2, E3 were used to study the solvent effect on INH crystal defects;
E3, E4, E5 were used to study the supersaturation effect on INH crystal defects in isopropanol;
E3, E6, E7 were used to study the stirring rate effect on INH crystal defects in isopropanol;
E3, E8, E9 were used to study the temperature effect on INH crystal defects in isopropanol.

(G_{hkl}) is proportional to the attachment energy (E^{att}_{hkl}):

$$G_{hkl} \propto E^{att}_{hkl} \quad (1)$$

where the attachment energy (E^{att}_{hkl}) is defined as the released energy by generating a growth slice on the growing. The attachment energy (E^{att}_{hkl}) is negatively related to the interaction energy (E_{int}) between the crystal surface layer and the solvent layer [28,29]. The interaction energy (E_{int}) can be obtained by the following formula.

$$E_{int} = E_{tot} - (E_{sur} + E_{sol}) \quad (2)$$

where E_{tot} represents the total energy of the INH crystal surface and the solvent interfacial system; E_{sur} and E_{sol} stand for the energy of the isolated crystal surface and the solvent respectively.

It can be seen that the relative growth rate of the ($h\ k\ l$) face (G_{hkl}) is inversely related to the interaction energy (E_{int}). In this work, the relation between G_{hkl} and E_{int} was used to reflect the role of the solvent in the crystal growth to further reveal the effect of solvents on the defects.

2.4.2. Computational details

We calculated the interaction energy (E_{int}) between the solvent (methanol, ethanol, and isopropanol) and the target crystal surface, namely (1 1 0) surface and (0 0 2) surface. These two crystal surfaces determine the INH crystal growth in the axial and radial directions, respectively [30].

The INH crystal used in calculation belonged to an orthorhombic crystal system with the space group P $2_12_12_1$ and unit cell dimensions of a = 3.8499 Å, b = 11.344 Å, c = 14.745 Å, Z = 4, which presents a similar structure to that by Lemmerer [31]. The INH crystal was cleaved parallel to the (0 0 2) or (1 1 0) surface with a thickness of around 40 Å. The chosen solvent was methanol, ethanol, or isopropanol. A solvent layer containing 400 or 450 solvent molecules was constructed by the Amorphous cell model. The two-layer interfacial model was used for molecular dynamics (MD) simulation to study the influence of solvent on crystal surfaces. In the two-layer interfacial model, the solvent layer was adsorbed on the (0 0 2) or (1 1 0) surface along the c axis. The vacuum slab of 120 Å thickness was built above the solvent layer to eliminate the effect of the additional free boundaries on the structure. The crystal slice was constrained during MD simulation. The interfacial model was geometrically optimized before the dynamic simulation. MD simulations were carried out in the NVT ensemble at the INH crystallization temperature of 298 K. The time step of MD simulation was 1 fs and the total simulation time of 50 ps was performed when the whole system reached a steady state.

In this study, all calculations were run using the commercial molecular modeling software package Materials Studio 5.0, using the COMPASS force field based on the Forcite module [28,29]. The van der Waals force and electrostatic force were calculated by the Atom-based and Ewald summation methods [32], respectively. The cutoff radius for the Atom-based method was set to 15.5 Å, while the accuracy of the Ewald method was 0.0001 kcal·mol^{-1}.

2.5. Single-crystal growth experiment

The single-crystal growth experiments were performed at different supersaturation to study the growth mechanism of INH crystals in isopropanol. The supersaturated solution was slowly evaporated at 298.15 K to obtain INH seeds with the size of 200 × 600 μm. As for the supersaturated solution preparation, INH crystals with a certain amount were dissolved in isopropanol at 303.15 K and then cooled to 298.15 K. The INH seed was placed on a jacket glass dish, and then about 20 mL of the supersaturated solution was put into the glass dish quickly. The temperature controller remained at 298. 15 K for crystal growth and the optical polarizing microscope was applied to monitor the change in INH crystal size at regular time intervals. The change in the axial and radial direction length divided by time was regarded as the growth rate of the axial and radial directions, respectively. Each experiment was repeated at least 5 times, and the average value was used as the final result.

2.6. Ultrasound

An ultrasonic homogenizer (Ningbo Xinzhi Biotechnology Co., Ltd.) was performed to sonicate the solution for one minute after cooling crystallization, and then the solution was stirred for 3 h. The ultrasonic power was set as 180 W, 315 W, 450 W, 585 W, and 720 W, respectively.

3. Results

3.1. Batch crystallization

3.1.1. Solvent effect

In methanol, ethanol, and isopropanol, INH crystals grew in a rod-like shape without polymorphs (PXRD evidence shown in Figure S1). In Fig. 2, the INH crystals obtained from methanol presented almost no defects; part of the crystals in ethanol had internal inclusions which mainly were distributed in the axial direction; while the crystals obtained in isopropanol exhibited defects in the axial and radial directions where some hollow cavities could be observed in the axial direction.

3.1.2. Crystallization operation parameters

Herein, the effects of crystallization operation parameters (temperature, supersaturation, stirring rate) on the defects of INH crystals in isopropanol were investigated in detail.

Temperature effect. As shown in Fig. 3, the INH defects in isopropanol increased with the increase in temperature. In detail, cavities appeared in the axial direction of crystals at moderate temperature (around 298.15 K). With the temperature increasing, there were not only cavities in the axial direction but also laminar fractured cavities in

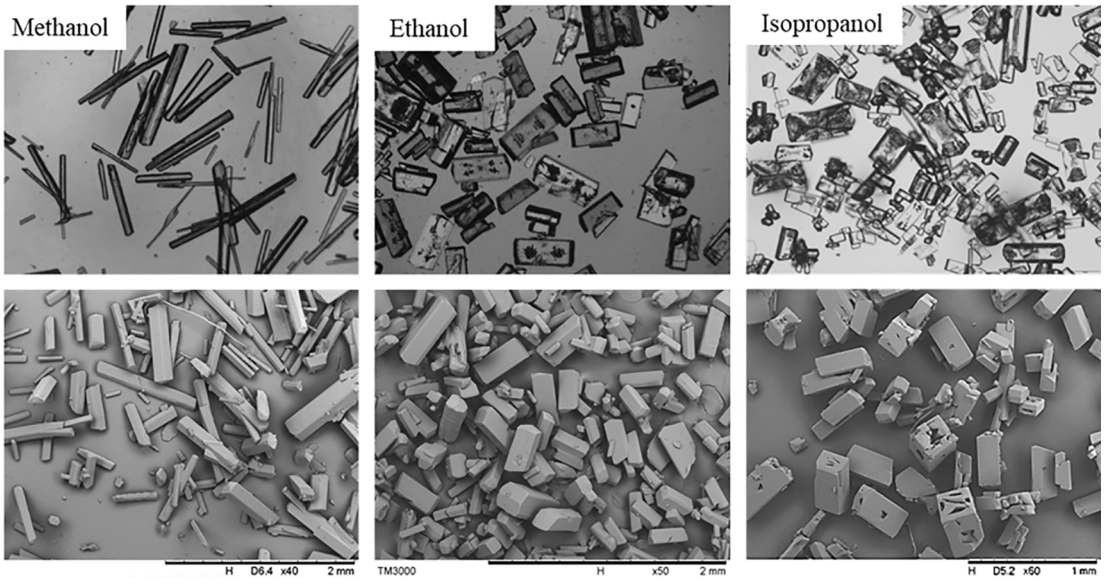

Fig. 2. Effect of solvent on INH crystal defects when $S = 1.5$, $T = 298.15$ K, and $r = 300$ rpm. (The three above are optical microscopic images while the three at the bottom are SEM images.)

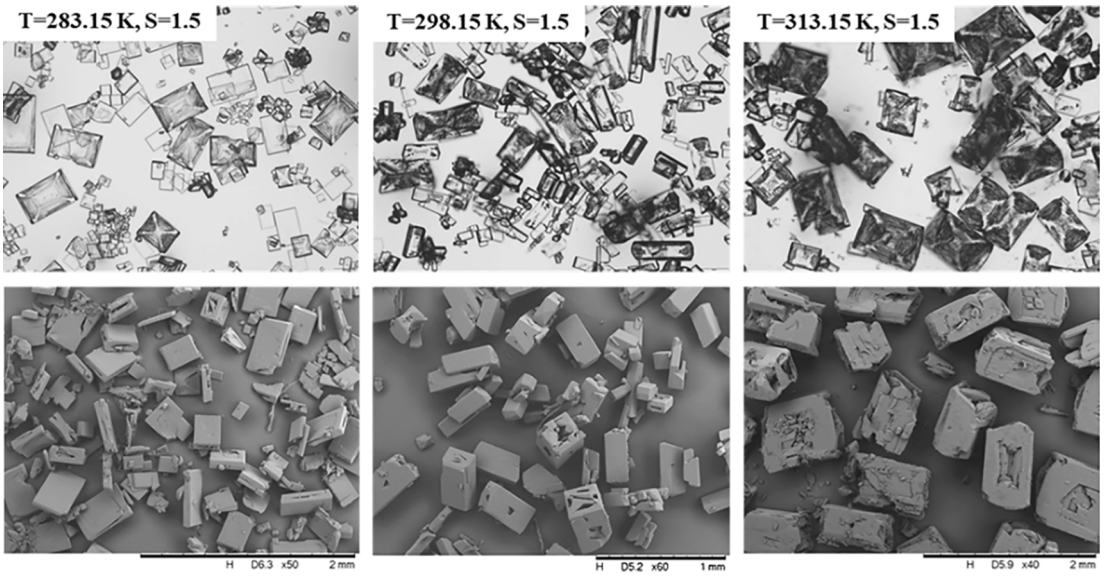

Fig. 3. Effect of temperature on INH crystal defects in isopropanol when $S = 1.5$ and $r = 300$ rpm. (The three above are optical microscopic images while the three at the bottom are SEM images.)

the radial direction.

Stirring rate. The relatively high stirring rate had an inhibitory effect on INH crystal defects (see Fig. 4). As the stirring rate increased, the crystal became smaller with fewer defects. Besides, the crystal aspect ratio and the particle size decreased with the increase of the stirring rate. Herein, we defined the aspect ratio (R) as the ratio of the longest and the shortest crystal dimensions.

Supersaturation. In Fig. 5, the formation of defects was negatively related to supersaturation. As the supersaturation increased, the number of crystals with defects became fewer while the crystals became thinner with a larger aspect ratio.

3.2. Molecular simulation

The (1 1 0) crystal surface and the (0 0 2) crystal surfaces shown in Fig. 6 determine the INH crystal growth of the axial direction and the radial direction respectively [30]. All the calculated interaction energies were listed in Table 2. The simulated interfaces were presented in Figure S2.

In Table 2, for the (1 1 0) surface, the interaction energy between the surface and methanol is the smallest while the interaction energy between the surface and ethanol is slightly larger than that between the surface and isopropanol, which means the affinity ability of methanol on the (1 1 0) surface is weak while that of ethanol or isopropanol on the (1 1 0) surface is strong. For the (0 0 2) surface, the interaction energy increases from methanol, ethanol to isopropanol, which illustrates that the affinity ability on the (0 0 2) surface increases from methanol, ethanol to isopropanol. Moreover, from Table 2, it can be found that the interaction energy between solvent and (0 0 2) surface is larger than that of the solvent and (1 1 0) surface, which infers that the affinity ability of solvent on the (0 0 2) surface is stronger and more energy is needed for the (0 0 2) surface to get the solvent desorbed.

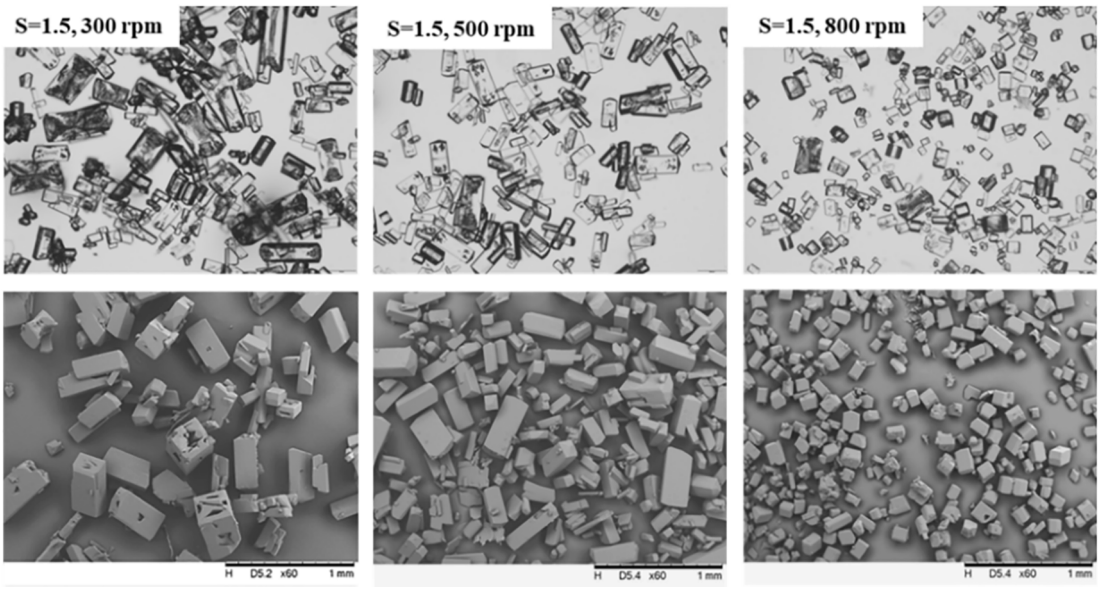

Fig. 4. Effect of stirring rate on INH crystal defects in isopropanol when $T = 298.25$ K and $S = 1.5$. (The three above are optical microscopic images while the three at the bottom are SEM images.)

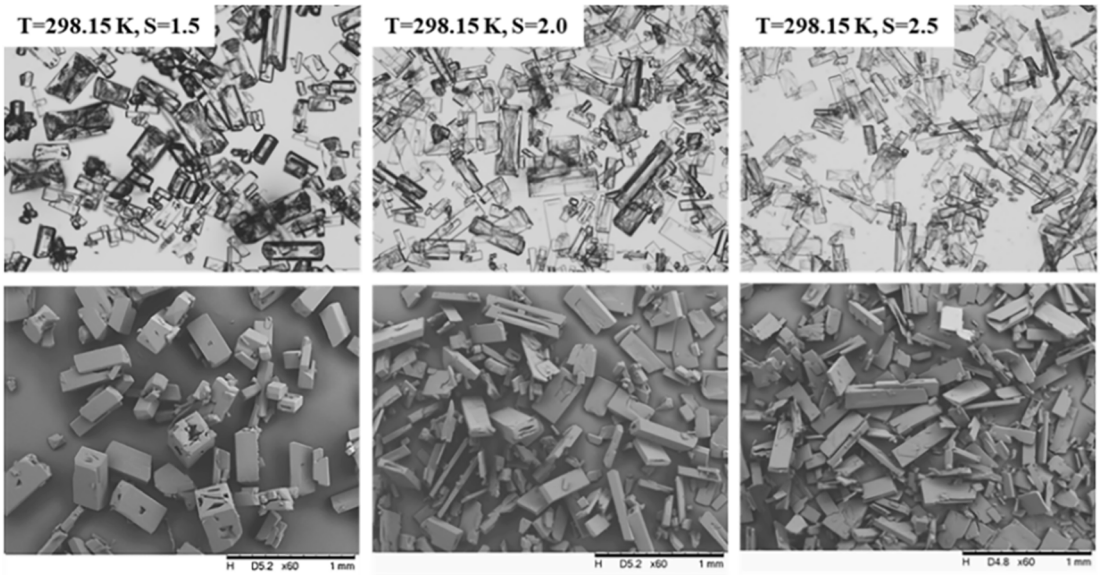

Fig. 5. Effect of supersaturation on crystal defects when $r = 300$ rpm and $T = 298.15$ K. (The three above are optical microscopic images while the three at the bottom are SEM images.)

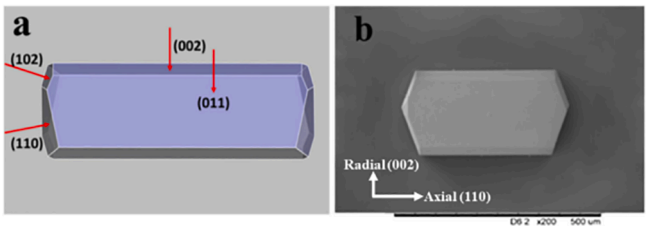

Fig. 6. (a) predicted INH in isopropanol by AE model (where main surfaces were labeled); (b) experimental INH crystal in isopropanol. (Modified from ref. 30.)

Table 2
The interaction energy between the solvent and the crystal surface.

Solvent Crystal surface	Methanol(E_{int}/ kcal•mol^{-1})	Ethanol(E_{int}/ kcal•mol^{-1})	Isopropanol(E_{int}/ kcal•mol^{-1})
(1 1 0)	−42310.156	−42268.263	−42286.376
(0 0 2)	−16381.542	−16317.544	−16291.530

3.3. Raman microscopy

The liquid inclusions as macroscopic defects refer to the area where is filled with liquid inside the crystal, which can affect the purity and mechanical property of crystals [33]. Raman microscopy is an effective tool to clarify the chemical composition of liquid inclusions without destruction [19,34,35].

The liquid inclusions in INH crystals were characterized by Raman microscopy. And the spectra of the liquid inclusion, the pure isopropanol, and bulk crystal were presented in Fig. 7. In detail, the spectrum of the liquid inclusion in Fig. 7a contained a characteristic peak of isopropanol at 816 cm^{-1} and a characteristic peak of INH crystals at 1325 cm^{-1}, which inferred that the liquid inclusions were composed of mother liquor.

3.4. N_2 adsorption–desorption measurement

We performed the N_2 adsorption–desorption measurement to semi-quantitatively characterize the cavity defects of INH crystals as the volume of N_2 adsorption reflected the severity of the cavities in INH crystals [19,36]. It should be noted that the cavities formed by the fracture of liquid inclusions and the growth cavities were both measured here.

The N_2 adsorption–desorption isotherms of the INH crystals obtained at different supersaturation, temperature, and stirring rates were shown in Fig. 8. The adsorption isotherms could approximately be identified as type III [37]. All the desorption curves almost coincided with the adsorption curves. In Fig. 8a, the gas adsorption capacity of the crystals increased with the increase in temperature, which inferred that the crystal surface defects increased as the temperature increased, which was consistent with the observation shown in Fig. 3. On the other hand, the gas adsorption capacity decreased as the stirring rate increased (see Fig. 8b), which indicated that the crystal surface defects decreased with the stirring rate increasing, which was coherent with the observation shown in Fig. 4. Besides, once the stirring rate was above 500 rpm, the gas adsorption was maintained at a certain value. Moreover, the gas adsorption capacity of INH crystals was negatively related to the

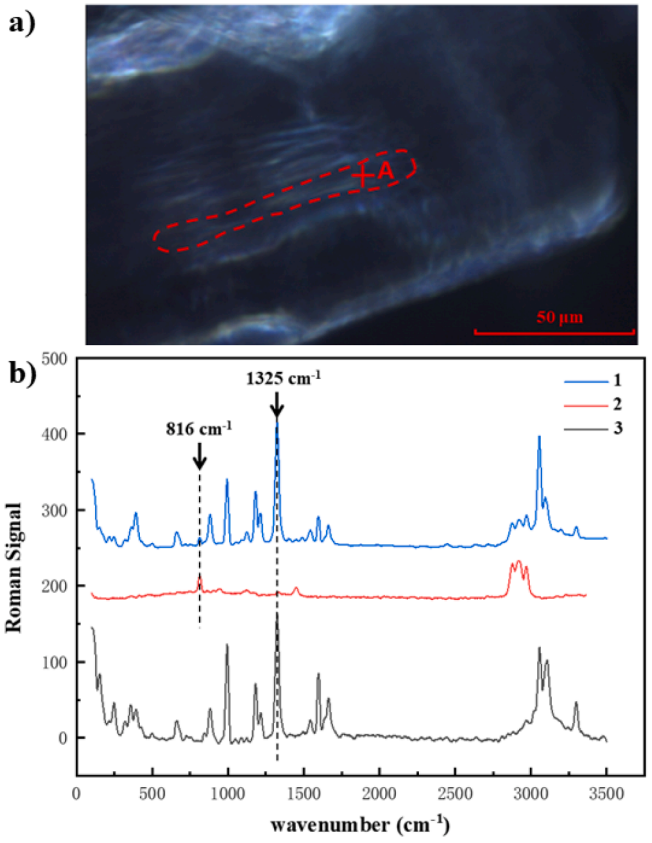

Fig. 7. (a) Optical microscopic image of the crystal where the Raman spectrum of the inclusion was obtained. (A is for the target defect and the circled area by dotted lines is the possible inclusion.); (b) Raman spectra of 1 for liquid inclusions inside INH crystals, 2 for pure isopropanol, and 3 for bulk crystals.

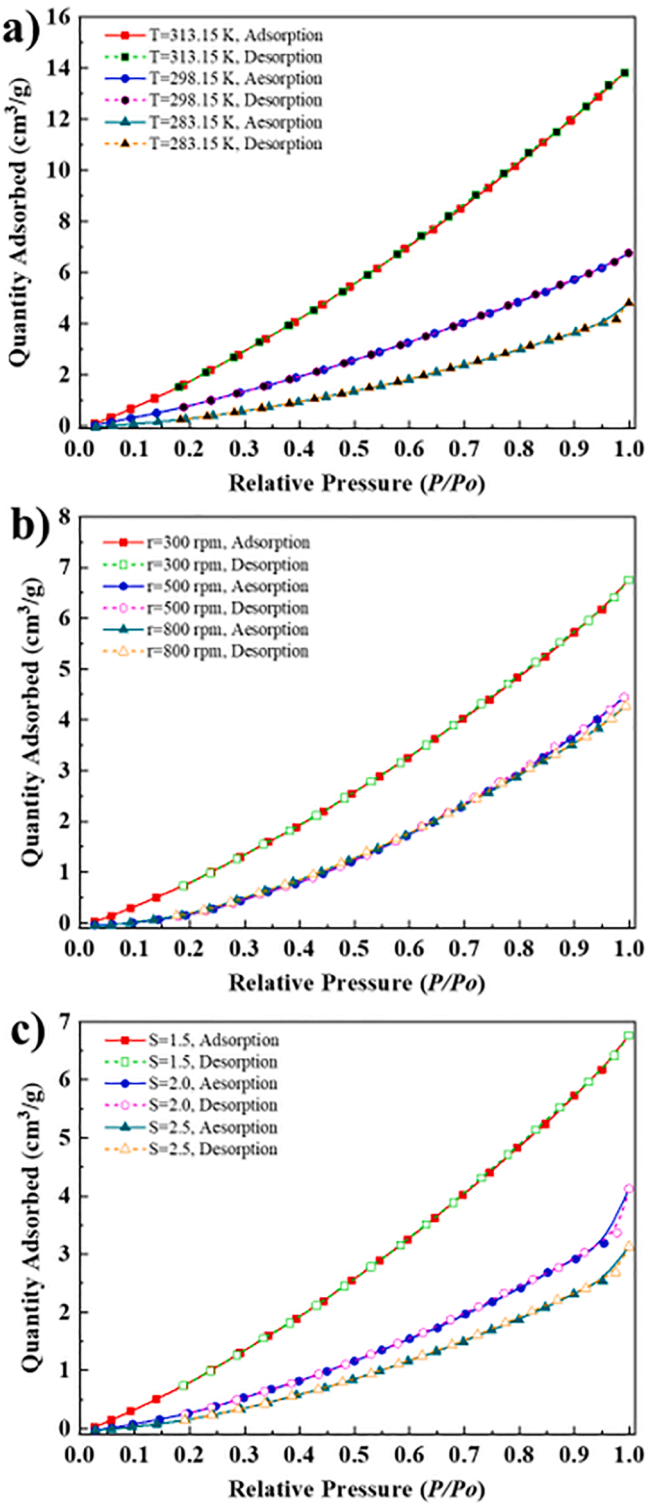

Fig. 8. N_2 adsorption–desorption isotherms of INH crystallized at different (a) crystallization temperatures, (b) stirring rates, and (c) supersaturation.

supersaturation (see Fig. 8c), which meant that the crystal surface defects tended to decrease as the supersaturation increased, which was in accord with the observation shown in Fig. 5. Interestingly, when comparing the effect of the three factors (temperature, stirring rate, and supersaturation) on the bulk defects in Fig. 8a-c, it can be found that high temperature (313.15 K) can lead to the most serious defects.

3.5. Single-crystal growth experiments

The single crystal growth experiment was carried out to figure out the growth mechanisms in the axial and radial directions and the axial and radial growth rates correspond to the growth rates of the (1 1 0) surface and (0 0 2) surface of INH crystals respectively.

It can be seen from Figs. 9-10 that the (1 1 0) crystal surface always had a slower growth rate compared to that of the (0 0 2) crystal surface. Besides, the two surfaces acted differently with the supersaturation. The growth rate of the axial (1 1 0) surface was approximately proportional to the supersaturation while the growth rate of the radial (0 0 2) crystal surface increases slightly with the increase of the supersaturation without the linear relationship. Interestingly, the relative growth rate of the two surfaces decreased slightly but turned up then. Due to the increase in the relative growth rate, the aspect ratio increased with the supersaturation, which was further proved by the morphologi G3 (the details are in the supporting information, shown in Figure S3 and S4).

3.6. Ultrasound

Herein, the ultrasound was used to modulate the crystal defects of INH crystals. The morphology of crystals obtained by carrying out an ultrasonic homogenizer under different powers (180 W, 315 W, 450 W, 585 W, and 720 W) was exhibited in Fig. 11. First of all, it was obvious that the crystal defects were significantly reduced under the action of ultrasound. Besides, there were still some defects under low ultrasonic power while crystals became smaller with crystal fragments under high power (more evidence shown in Figure S5). So, there existed an optimal ultrasonic power to obtain defect-free crystals with appropriate size. In our case, INH crystals with the best morphology were obtained at 450 W of an ultrasonic homogenizer (see Fig. 11d). It should be noted that ultrasound was an external physical field without the transformation of INH crystal forms (see Figure S6).

4. Discussion

4.1. Growth mechanisms of INH crystals

According to the kink sites theory [38–40] (kink sites refer to the exposed trihedral corners on a crystal surface where molecules are most readily incorporated into or get detached from the lattice), the process of crystal growth can be divided into three steps; (a) bulk diffusion during which the growth units are transported from the bulk solution; (b) surface integration during which solvent molecules get desorbed while solute molecules are incorporated into kink sites; (c) heat transport with the release and transport of the latent heat. The growth rate of a crystal surface is limited by the slowest step of these processes that is the determining step of the crystal growth [40].

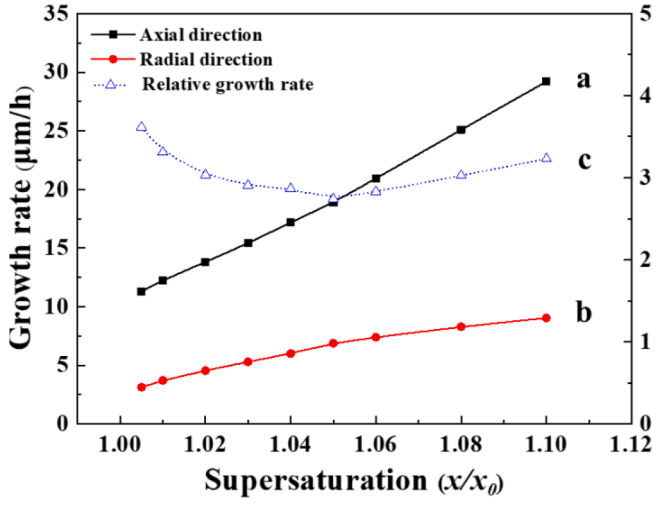

Fig. 9. Crystal growth rates of INH crystal along (a) axial direction, and (b) radial direction, and (c) relative growth rate of axial and radial direction at different supersaturations.

From the single crystal growth experiment, for the (1 1 0) surface, the growth rate accelerated as the supersaturation increased, which indicated that the growth rate of the (1 1 0) surface linearly depends on the number of solute molecules near the surface. Moreover, the number of solute molecules is directly related to bulk diffusion, which means that the growth of the (1 1 0) surface is directly related to bulk diffusion. Therefore, it can be concluded that the growth of the axial (1 1 0) surface obeys the rough growth mechanism whose determining step is the bulk diffusion [30].

Unlike the (1 1 0) surface, the radial (0 0 2) surface grew slowly without a linear relationship with supersaturation. It should be noted that the (0 0 2) surface is a polar surface, in which the pyridine nitrogen and the amide functional group of the INH molecule are exposed to the solution. Thereby, the (0 0 2) surface can be growth-inhibited due to the high interaction with the polar solvent. In conclusion, the growth of the (0 0 2) surface is restricted by the surface integration, which conforms to the stepwise growth mechanism [30].

4.2. Formation mechanism of crystal defects

It can be seen from the above work that cavities mainly appeared in the axial direction of the crystals while liquid inclusions mainly existed in the radial direction of the crystals. Moreover, variations of defects in the two directions were not consistent. Thus, we inferred that the defects in the two directions have different formation mechanisms. Moreover, considering the importance of the (1 1 0) surface and the (0 0 2) surface in the axial and radial directions [30], we approximated the axial and radial defects to occur on the (1 1 0) surface and (0 0 2) surface, respectively.

4.2.1. Cavities

For INH crystals, cavities were mainly formed in the axial (1 1 0) surface which can be directly seen in the optical microscopic images and SEM images. For the rough growth of the (1 1 0) surface, bulk diffusion is the determining step. Nevertheless, according to the starvation phenomenon proposed by E. Roedder [41], INH molecules are more likely to diffuse to the crystal corners and edges than the center of the surface. The phenomenon causes a concentration gradient from the corners and edges to the surface center, i.e. the high local supersaturation near the crystal surface. Thus, as the growth rate of the crystal edges is greater than that of the center, edges grow higher to prevent the solute from spreading to the center, thereby inhibiting the growth of the center and forming a cavity (Fig. 12).

Based on the formation mechanism of defects in the (1 1 0) surface above, the reasons for the formation of crystal defects can be explained. For the effect of solvents on the (1 1 0) surface, cavities appeared in isopropanol but no defects in methanol, which resulted from the interaction between the solvent and the crystal surface that was reflected by the calculated interaction energy in Table 2. In detail, strong interaction between isopropanol and INH hampers the diffusion of solute molecules, thereby impeding the growth of the (1 1 0) surface, which in turn explains that the crystal seems to be defect-free in methanol (the defects in ethanol will be discussed later). Besides, the interaction can explain the reason for the more rapid growth of the (1 1 0) surface than that of the (0 0 2) surface since the interaction energy between solvent and the (1 1 0) surface is less than that of the (0 0 2) surface.

When the temperature, the stirring rate, and the supersaturation of the solution were changed, the defects in the (1 1 0) surface changed differently. On the one hand, increasing the temperature of the system accelerates the diffusion of the solutes, which aggravates the local supersaturation near the (1 1 0) surface, thereby making the defects more

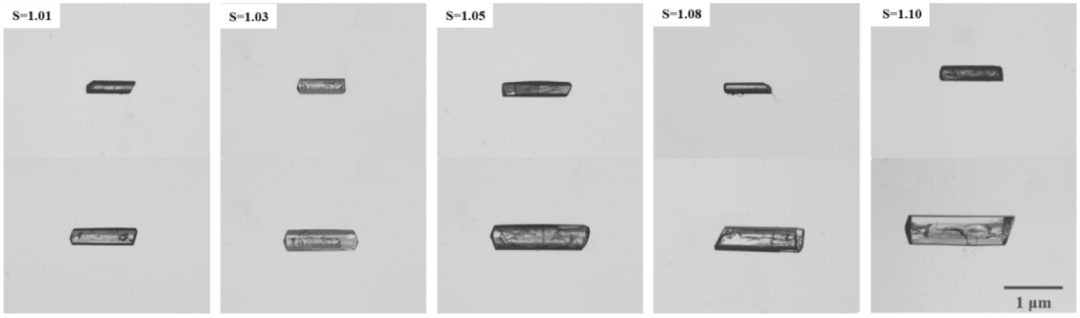

Fig. 10. Morphological evolution of growing INH seed crystal in isopropanol at different supersaturations in 24 h.

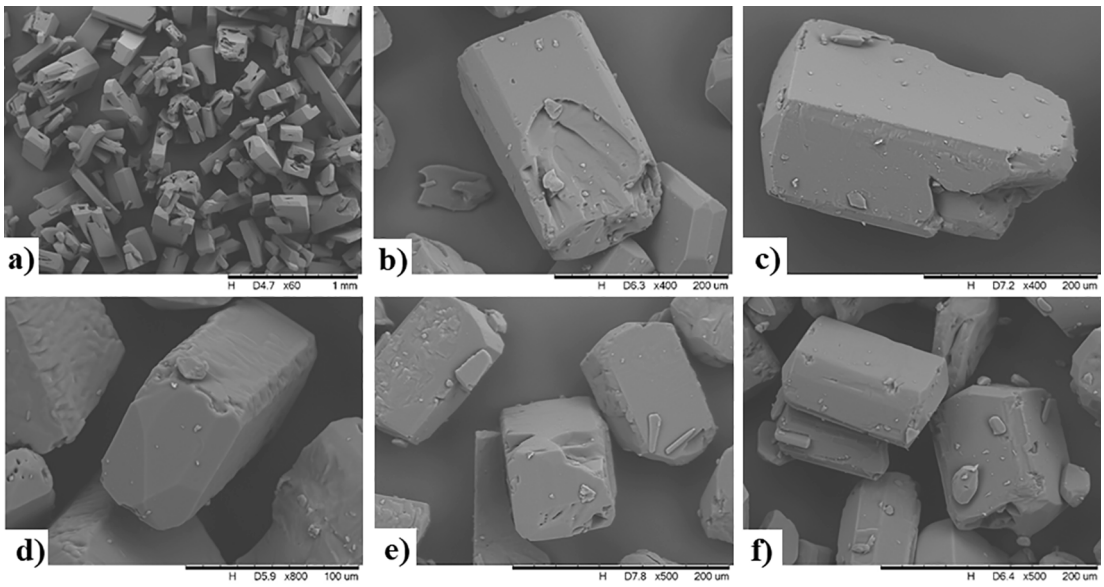

Fig. 11. SEM images of INH crystal (a)without ultrasound, at (b) 180 W, (c) 315 W, (d) 450 W, (e) 585 W, and (f) 720 W of ultrasound.

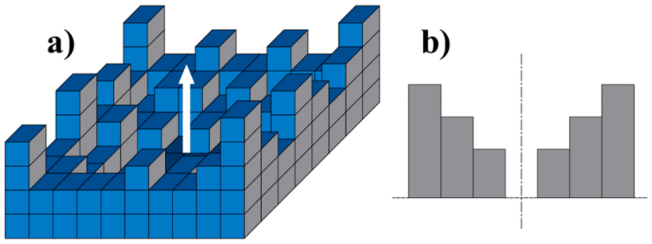

Fig. 12. (a) Visual model for the rough growth when forming a cavity (the white arrow represents the growth direction, and the cubes represent the solute molecules); (b) simplified profile of the cross-sectional rough growth. The solvent molecules are hidden.

serious, as shown in Fig. 3. On the other hand, the rising stirring rate promotes uniform supersaturation, which compensates for the local supersaturation near the (1 1 0) surface. Therefore, defects are reduced (see Fig. 4). Similarly, as the supersaturation of the solution system increases, defects are not easy to form with enough solute molecules near the surface (see Fig. 5).

4.2.2. Liquid inclusions

In section 3, the opaque internal defects shown in the optical microscopic images and the layered fractured structure observed in the SEM images indicated the liquid inclusions mainly exist in the radial (0 0 2) surface. Furthermore, the existence of liquid inclusions was verified by Raman microscopy which was shown in section 3.4. According to the stepwise growth mechanism of the (0 0 2) surface, surface integration is the determining step that limits the growth rate. During the surface integration, the solvent molecules get detached from the surface while the solute molecules are inserted into the kink sites. The solute insertion rate competes with the solvent removal rate. As shown in Fig. 13, when the solute insertion rate of the latter layer is greater than the solvent removal rate, the solvent molecules of the former layer which are adsorbed on the crystal surface can be trapped to form a liquid inclusion in the (0 0 2) surface.

Based on the formation mechanism of defects in the (0 0 2) surface above, the reasons for the factors affecting defects in the radial direction can also be explained. The effect of the solvent on the crystal defects is

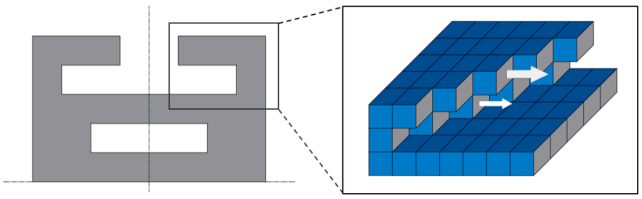

Fig. 13. Visual model of the stepwise growth when forming a liquid inclusion. The left is the simplified profile of the cross-sectional stepwise growth and the right is the locally amplified visual model for the rough growth when forming a cavity. The white arrow represents the stacking direction of the growth units, and the cubes represent the solute molecules while the solvent molecules are hidden.

due to the interaction between the solvent and the crystal surface. In detail, when the interaction between the solvent and the (0 0 2) surface is strong, the removal rate of the solvent is smaller than the solute insertion rate, which results in liquid inclusions. Moreover, it can be seen in Table 2, the interaction between isopropanol and the (0 0 2) surface is the strongest, which causes the most serious inclusions in INH crystals as shown in Fig. 2.

For the (0 0 2) surface, temperature promotes the diffusion of solutes, thereby increasing the solute insertion rate and then enlarging the gap between the solute insertion rate and the solvent removal rate. As a result, the solvent molecules are intercepted in the crystal to form inclusions. It is consistent with the serious phenomenon of inclusions at the high temperature in Fig. 3. On the other hand, the increase of the stirring rate makes the solution system mixed more uniformly, so the solute insertion rate and solvent removal rate on the (0 0 2) surface approach each other without inclusions formed (see Fig. 4). Similarly, as supersaturation increases, there are sufficient solute molecules near the (0 0 2) surface, which in turn means that there are not enough solvent molecules nearby; thereby, it is hard to form inclusions (see Fig. 5).

On the other hand, for the special case of liquid inclusions in the (1 1 0) surface obtained in ethanol (Fig. 2), the hypothetical process is that ethanol presented the highest interaction energy with the (1 1 0) surface is hard to be removed and then trapped in the surface when the fast growth comes from the edges and corners to the surface center, ending with the liquid inclusions.

4.3. Approaches for inhibiting crystal defects

The defects of INH crystals such as cavities and liquid inclusions are unfavorable, which can reduce the purity and stability of the INH crystals. It is necessary to eliminate the defects of INH crystals. Based on the formation mechanism of INH crystal defects above, we analyzed the effect of crystallization operation parameters on overall defects and then, proposed an effective method of ultrasound to reduce INH crystal defects.

4.3.1. Crystallization operation parameters

The crystallization operation parameters (temperature, stirring rate, and supersaturation) have consistent effects on the axial and radial defects of INH crystals, which are that an appropriate decrease in temperature and a proper increase in stirring rate and supersaturation can reduce the formation of defects.

We semi-quantitatively reflected the influence of these three parameters on the overall defects through the N_2 adsorption–desorption measurement, which offered a good reference to reduce crystal defects by adjusting the crystallization parameters.

In the overall Fig. 8, the isotherms did not have a hysteresis loop as the desorption curves almost coincided with the adsorption curves, which reflected the large size of the cavities. Then, comparing Fig. 8a-c, it can be seen that high temperature can enhance crystal defects, so the high temperature should be avoided in the production process of INH; besides, increasing the stirring rate or increasing the supersaturation can effectively reduce the defects of INH crystals. However, the rising-up of the stirring rate significantly decreases the crystal size which may further make the crystals prone to aggregation (see Fig. 4); besides, the increase in supersaturation can result in thin crystals which are difficult to store (see Fig. 5). Therefore, other approaches should be proposed to obtain crystals with good morphology and few defects.

4.3.2. Ultrasound

Ultrasound is an effective method to reduce the growth defects of INH crystals (see Fig. 11). Herein, we carried out an ultrasonic homogenizer at 450 W to obtain INH crystals with the best morphology and the least defects. Also, regardless of the power, crystal defects can be improved by the presence of ultrasound. To be more enlightening for the ultrasonic strategy of defect elimination, we analyzed the effect of ultrasound on the formation process of INH crystal defects based on the defect formation mechanism.

When ultrasonic waves propagate in a liquid medium, the energy of ultrasonic waves is the driving force for mass transfer and triggers the formation and implosion of cavitation bubbles, which is named “cavitation” [42]. In detail, under the negative pressure of sound waves, cavitation bubbles composed of vapor and dissolved gases are generated. Then, the bubbles implode violently, forming a local hot spot with high local temperature and pressure, and releasing a powerful shock wave. This is a very fast process that can induce nucleation [23,43]. Besides, local hot spots might affect the crystal lattice, and the abrasion caused by shock waves makes the crystal size of the product smaller [44].

In our case, for the (1 1 0) surface that follows the rough growth mechanism, the implosion of cavitation bubbles caused by ultrasound makes the solution well mixed, which compensates the local supersaturation [45], and reduces the growth rate of the corners and ridges to approach the growth rate of the crystal surface center. Hence, the growth of the crystal surface is relatively uniform, and defects are not easy to form.

For the (0 0 2) surface that follows the stepwise growth mechanism, the cavitation phenomenon formed by ultrasound causes large-scale nucleation [46], which then consumes solute molecules, and decreases the solute insertion rate on the crystal surface. Furthermore, the solution is well mixed by ultrasound that slightly increases the removal rate of the solvent on the crystal surface. Therefore, the difference between the solute insertion rate and the solvent desorption rate is shortened, which reduces the liquid inclusions.

5. Conclusion

In this paper, the growth defects of INH crystals were systematically studied which may provide a theoretical basis for the preparation of perfect INH crystals with high purity and few defects. Through experiments and molecular simulation, strong interaction between the solvent and the crystal surface, high temperature, low supersaturation, and low stirring rate can contribute to serious growth defects in INH crystals. The formation mechanism of INH crystal defects was first proposed based on the crystal growth mechanism. In the axial rough growth, i.e. the (1 1 0) surface, due to the starvation phenomenon of solute diffusion, the growth rate of the crystal edges is greater than that of the center, thereby forming a cavity in the surface. On the other hand, in the radial stepwise growth, i.e. the (0 0 2) surface, when the solvent removal rate is smaller than the solute insertion rate, the crystal surface is solvent-encapsulated to form liquid inclusions.

Furthermore, ultrasound-assisted crystallization was performed to reduce the INH crystal defects, and defect-free INH crystals were successfully obtained at 450 W of an ultrasonic homogenizer. Besides, the affecting process of ultrasound was well explained based on the formation mechanism of crystal defects. Overall, the formation mechanism of INH defects can be an inspiration for the preparation of perfect isoniazid products. The hypothetical formation process of defects can guide the adjustment of crystallization operation parameters. Moreover, the defect elimination strategy based on ultrasound provides an effective scheme to get perfect crystals.

CRediT authorship contribution statement

Min Li: Writing - original draft, Methodology, Formal analysis, Software. **Weiguo Hu:** Resources. **Lingyu Wang:** Validation. **Jiahao Wei:** Data curation. **Jingjing Sun:** Visualization. **Jiahui Li:** Investigation. **Dandan Han:** Conceptualization, Writing - review & editing. **Junbo Gong:** Project administration, Funding acquisition.

Declaration of Competing Interest

The authors declare that they have no known competing financial interests or personal relationships that could have appeared to influence the work reported in this paper.

Acknowledgment

This work was supported by the Chemistry and Chemical Engineering Guangdong Laboratory (Grant No. 1912014).

Appendix A. Supplementary data

Supplementary data to this article can be found online at https://doi.org/10.1016/j.ultsonch.2021.105674.

References

[1] R. Ray, A.M. Srivastava, Measuring cosmic defect correlations in liquid crystals, Phys. Rev. D 69 (2004), 103525.
[2] V. Ehrlacher, C. Ortner, A.V. Shapeev, Analysis of boundary conditions for crystal defect atomistic simulations, Arch. Ration. Mech. Anal. 222 (3) (2016) 1217–1268.
[3] A. Waldschmidt, V. Dupray, B. Berton, N. Couvrat, S. Petit, G. Coquerel, Incidence of crystal growth conditions on the formation of macroscopic liquid inclusions in ciclopirox crystals, J. Cryst. Growth 342 (1) (2012) 72–79.
[4] G. Staikov, W.J. Lorenz, The role of crystal imperfections in electrochemical phase formation and growth, Can. J. Chem. 75 (11) (1997) 1624–1634.
[5] M.M. Islam, S. Pola, Y.-T. Tao, High mobility n-channel single-crystal field-effect transistors based on 5,7,12,14-tetrachloro-6,13-diazapentacene, Chem. Commun. 47 (22) (2011) 6356, https://doi.org/10.1039/c1cc11762a.
[6] S. Conesa-Boj, I. Zardo, S. Estradé, L.i. Wei, P. Jean Alet, P. Roca i Cabarrocas, J. R. Morante, F. Peiró, A.F.i. Morral, J. Arbiol, Defect formation in Ga-catalyzed silicon nanowires, Cryst. Growth Des. 10 (4) (2010) 1534–1543.
[7] J.R. Toledo, K. Krambrock, Identification and thermal stability of point defects in neutron-irradiated hexagonal boron nitride (h-BN), J. Phys. D: Appl. Phys. 54 (2021), 065303.
[8] R. Li, W. Hu, Y. Liu, D. Zhu, Micro- and nanocrystals of organic semiconductors, Acc. Chem. Res. 43 (4) (2010) 529–540.
[9] A. Folger, P. Ebbinghaus, A. Erbe, C. Scheu, Role of vacancy condensation in the formation of voids in rutile TiO_2 nanowires, ACS Appl. Mater. Interfaces 9 (15) (2017) 13471–13479.
[10] J.-W. Kim, J.-K. Kim, H.-S. Kim, K.-K. Koo, Characterization of liquid inclusion of RDX crystals with a cooling crystallization, Cryst. Growth Des. 9 (6) (2009) 2700–2706.
[11] D.D. Medina, Y. Mastai, Synthesis of DL-alanine mesocrystals with a hollow morphology, Cryst. Growth Des. 8 (2008) 3646–3651.
[12] L. Aisling, R. Åke, Crystal growth of single salicylamide crystals, Cryst. Growth Des. 19 (12) (2019) 7230–7239.
[13] K.G. Denbigh, E.T. White, Studies on liquid inclusions in crystals, Chem. Eng. Sci. 21 (9) (1966) 739–753.
[14] G.G.Z. Zhang, D.J.W. Grant, Formation of liquid inclusions in adipic acid crystals during recrystallization from aqueous solutions, Cryst. Growth Des. 5 (1) (2005) 319–324.
[15] N. Couvrat, A.S. Blier, B. Berton, Y. Cartigny, V. Dupray, G. Coquerel, Characterization of defects inside single crystals of ciclopirox, Cryst. Growth Des. 9 (6) (2009) 2719–2724.
[16] A. Waldschmidt, I. Rietveld, N. Couvrat, V. Dupray, M. Sanselme, B. Berton, B. Nicolai, N. Mahé, S. Petit, R. Céolin, G. Coquerel, About aged heterogeneous liquid inclusions inside organic crystals in relation to crystal formation, structure, and morphology, Cryst. Growth Des. 11 (6) (2011) 2580–2587.
[17] A. Waldschmidt, N. Couvrat, B. Berton, V. Dupray, S. Morin, S. Petit, G. Coquerel, Impact of gas composition in the mother liquor on the formation of macroscopic inclusions and crystal growth rates. Case study with ciclopirox crystals, Cryst. Growth Des. 11 (6) (2011) 2463–2470.
[18] P. Sun, Y. Wang, S. Rohani, E. Liu, S. Du, S. Xu, M. Chen, Z. Wei, J. Gong, Controlled recrystallization of tubular vinpocetine crystals with increased aqueous dissolution rate and In vivo bioavailability, Cryst. Growth Des. 17 (11) (2017) 5790–5800.
[19] Z. Yu, Y. Wang, S. Du, J. Zhou, L. Zhou, Impact of affecting the formation defects in vinpocetine crystals, Cryst. Growth Des. 20 (5) (2020) 3093–3103.
[20] N. Amara, B. Ratsimba, A.-M. Wilhelm, H. Delmas, Crystallization of potash alum: effect of power ultrasound, Ultrason. Sonochem. 8 (3) (2001) 265–270.
[21] N. Lyczko, F. Espitalier, O. Louisnard, J. Schwartzentruber, Effect of ultrasound on the induction time and the metastable zone widths of potassium sulphate, Chem. Eng. J. 86 (3) (2002) 233–241.
[22] A.A. Thorat, S.V. Dalvi, Ultrasound-assisted modulation of concomitant polymorphism of curcumin during liquid antisolvent precipitation, Ultrason. Sonochem. 30 (2016) 35–43.
[23] C. Fang, W. Tang, S. Wu, J. Wang, Z. Gao, J. Gong, Ultrasound-assisted intensified crystallization of L-glutamic acid: Crystal nucleation and polymorph transformation, Ultrason. Sonochem. 68 (2020) 105227, https://doi.org/10.1016/j.ultsonch.2020.105227.
[24] S.R. Iyer, P.R. Gogate, Ultrasound assisted crystallization of mefenamic acid: Effect of operating parameters and comparison with conventional approach, Ultrason. Sonochem. 34 (2017) 896–903.
[25] S. Ramaswamy, J.M. Musser, Molecular genetic basis of antimicrobial agent resistance in Mycobacterium tuberculosis: 1998 update, Tubercle 79 (1998) (1998) 3–29.
[26] D.D. Han, B. Yu, Y.M. Liu, S.C. Du, S. Rohani, T. Zhang, S.Y. Liu, P. Shi, H.S. Wang, L.N. Zhou, J.B. Gong, Effects of additives on the morphology of thiamine nitrate: The great difference of two kinds of similar additives, Cryst. Growth Des. 18 (2018) 775–785.
[27] D. Han, T. Karmakar, F. Liu, Y. Wang, W. Tang, J. Gong, Uncovering the role of surfactants in controlling the crystal growth of pyridoxine hydrochloride, Cryst. Growth Des. 19 (12) (2019) 7240–7248.
[28] X. Duan, C. Wei, Y. Liu, C. Pei, A molecular dynamics simulation of solvent effects on the crystal morphology of HMX, J. Hazard. Mater. 174 (1-3) (2010) 175–180.
[29] L. Song, L. Chen, J. Wang, F. Chen, G. Lan, Prediction of crystal morphology of 3,4-Dinitro-1H-pyrazole (DNP) in different solvents, J. Mol. Graphics Modell. 75 (2017) 62–70.
[30] D. Han, T. Karmakar, Z. Bjelobrk, J. Gong, M. Parrinello, Solvent-mediated morphology selection of the active pharmaceutical ingredient isoniazid: Experimental and simulation studies, Chem. Eng. Sci. 204 (2019) 320–328.
[31] A. Lemmerer, Covalent assistance to supramolecular synthesis: modifying the drug functionality of the antituberculosis API isoniazidin situ during co-crystallization with GRAS and API compounds, CrystEngComm 14 (2012) 2465–2478.
[32] P.P. Ewald, Die Berechnung optischer und elektrostatischer Gitterpotentiale, Ann. Phys. (Berlin, Ger.) 369 (1921) 253–287.
[33] S. Yan, C. Xie, X. Zhang, L. Zhou, B. Hou, J. Huang, L. Zhou, Q. Yin, Influence of crystal growth conditions on formation of macroscopic inclusions inside thiourea crystals, Chemistryselect 3 (8) (2018) 2293–2297.
[34] S. Grishina, P. Koděra, S. Goryainov, A. Oreshonkov, Y. Seryotkin, F. Šimko, A. G. Polozov, Application of Raman spectroscopy for identification of rinneite ($K_3NaFeCl_6$) in inclusions in minerals, J. Raman Spectrosc. 51 (12) (2020) 2505–2516.
[35] G.M. Arzumanyan, A.S. Gur'ev, D.E. Kravtsunova, K.Z. Mamatkulov, A. S. Marchenko, K.A. Vereshchagin, A.Y. Volkov, Micro Raman spectroscopy for NETosis detection, J. Raman Spectrosc. 51 (10) (2020) 1960–1969.
[36] S. Brunauer, P.H. Emmett, E. Teller, Adsorption of gases in multimolecular layers, J. Am. Chem. Soc. 60 (2) (1938) 309–319.
[37] T.S. van Erp, J.A. Martens, A standardization for BET fitting of adsorption isotherms, Microporous Mesoporous Mater. 145 (1-3) (2011) 188–193.
[38] W.K. Burton, N. Cabrera, F.C. Frank, The growth of crystals and the equilibrium structure of their surfaces, Philos. Trans. R. Soc. Lond. A 243 (1951) 299–358, https://doi.org/10.1098/rsta.1951.0006.
[39] D.P. Woodruff, How does your crystal grow? A commentary on Burton, Cabrera and Frank (1951) 'The growth of crystals and the equilibrium structure of their surfaces', Philos. Trans. R. Soc. A 373 (2039) (2015) 20140230, https://doi.org/10.1098/rsta.2014.0230.
[40] M.A. Lovette, A.R. Browning, D.W. Griffin, J.P. Sizemore, R.C. Snyder, M. F. Doherty, Crystal shape engineering, Ind. Eng. Chem. Res. 47 (24) (2008) 9812–9833.
[41] E. Roedder, K.W. Howard, Fluid inclusions in salton sea scientific drilling project core: Preliminary results, J. Geophys. Res. 93 (B11) (1988) 13159–13164.
[42] S. Nalesso, M.J. Bussemaker, R.P. Sear, M. Hodnett, J. Lee, A review on possible mechanisms of sonocrystallisation in solution, Ultrason. Sonochem. 57 (2019) 125–138.
[43] K. Renuka Devi, A. Raja, K. Srinivasan, Ultrasound assisted nucleation and growth characteristics of glycine polymorphs–a combined experimental and analytical approach, Ultrason. Sonochem. 24 (2015) 107–113.
[44] S. Nii, S. Takayanagi, Growth and size control in anti-solvent crystallization of glycine with high frequency ultrasound, Ultrason. Sonochem. 21 (3) (2014) 1182–1186.
[45] J. Jia, W. Wang, Y. Gao, Y. Zhao, Controlled morphology and size of curcumin using ultrasound in supercritical CO_2 antisolvent, Ultrason. Sonochem. 27 (2015) 389–394.
[46] T. Hazi Mastan, M. Lenka, D. Sarkar, Nucleation kinetics from metastable zone widths for sonocrystallization of l-phenylalanine, Ultrason. Sonochem. 36 (2017) 497–506.